Pyrophyllite clay: led to preparing a porous geopolymers for removal of methylene blue from aqueous solutions

Youssef Ettahiri [a], Lahcen Bouna [a,*], John V. Hanna[b,*], Abdeljalil Benlhachemi [a], Hannah L. Pilsworth[b], Abdessalam Bouddouch [c] and Bahcine Bakiz [a]

[a] Materials and Environment Laboratory (LME), Faculty of Sciences, Ibn Zohr University, Dakhla City B.P. 8106, Agadir, Morocco.

[b] Department of Physics, University of Warwick, Coventry, CV4 7AL, United Kingdom.

[c] Reactivity and Chemistry of Solids Laboratory (LRCS) UMR CNRS/UPJV 7314, University of Picardy Jules Verne, France.

*** Lahcen BOUNA: E-mail: bounalahcen@gmail.com; Tel (+212673700422)**

*** John V. Hanna: E-mail: J.V.Hanna@warwick.ac.uk**

Abstract

This study reports the synthesis and characterization of a porous geopolymer systems based a naturally occurring Moroccan pyrophyllite clay. The contribution of pyrophyllite in geopolymerization reaction was very low, the geopolymer matrix formed was assured by alkaline activation of the metakaolin present in the sample. The pyrophyllite role is forming of disordered and heterogeneous geopolymer promote the pore creation. The structure and morphology of the raw natural clay, calcined meta-pyrophyllite phase and prepared geopolymer samples are characterized by several methods namely, X-ray Diffraction (XRD), ^{29}Si and ^{27}Al magic-angle-spinning nuclear magnetic resonance (MAS NMR) analysis, Fourier Transform Infra-Red (FTIR) spectroscopy, Differential Thermal Analysis (DTA) and Thermal Gravimetric Analysis (TGA), N_2 adsorption/desorption isotherm analysis by the Brunauer-Emmett-Teller (BET) method and Scanning Electron Microscopy (SEM). The specific surface area (S_{BET}) and pore volume (Vp) measured from products utilizing the calcined meta-pyrophyllite precursor (S_{BET} = 86 m^2/g and Vp = 0.08 cm^3/g) have both increased markedly compared to those values determined using a raw pyrophyllite clay phase (S_{BET} = 30 m^2/g and Vp = 0.05 cm^3/g). The methylene blue (MB) molecular adsorption experiment realized in water medium exhibited Pseudo Second Order (PSO) rate kinetics and adopted a Langmuir adsorption

model. The thermodynamics data shows that the chemisorption is spontaneous, irreversible and endothermic, with the quantity of MB molecules retained by the porous geopolymer specimen reaching 64.10 mg/g.

Keywords: Natural Pyrophyllite, Porous geopolymer, alkaline activation solution, adsorption, methylene blue.

1. Introduction

Geopolymers (inorganic polymers) are amorphous material based alkali aluminosilicates possessing a three-dimensional network structure that are produced by the alkali activation of silicon and aluminum rich sources such as clay minerals, fly ash, etc. (Davidovits, 1991; Darmayanti et al., 2019; Niu et al., 2022). Sodium silicate and alkali hydroxide (KOH and NaOH) are most commonly used to activate the silicon and aluminum species for the synthesis of geopolymer products (Longhi et al., 2020). In recent years, many studies have been devoted to these materials owing to their very interesting physicochemical characteristics. The chemical stoichiometric formulation ratios governing geopolymer formation (i.e. Si:Al; X:Al and H_2O:X_2O (X = Na, K) profoundly influence their properties (Zhang et al., 2014). Kaolinite ($Al_2Si_2O_5(OH)_4$) is 1:1 layered aluminosilicate mineral clay (i.e. atomic ratio Si:Al = 1) commonly used in geopolymer production. To attain the Si:Al formulation ratios of conventional geopolymers which reside in the range Si/Al = 2 - 4, it is necessary to augment the desired Si and Al inventory using alkaline activation solutions containing generally chemical products such as fly ash or other inorganic slag materials that are rich Si and Al rich. An alternative approach is to consider using clays such as pyrophyllite ($Al_2Si_4O_{10}(OH)_2$) which is a 2:1 layered aluminosilicate mineral clay (i.e. atomic ratio Si:Al = 2) which possesses a Si:Al ratio closer to the target geopolymer compositions in comparison to kaolinite clay. This method allows for a more economical rationalization of the Si-containing chemical precursors used for preparation of the alkaline activation solution thus reducing the cost of the geopolymer production.

The geopolymers have many applications in different fields such as construction material (Samuel et al., 2021), ceramics (Davidovits, 1991) and porous media used for pollutant adsorption from aqueous environments (Khan et al., 2015; Singhal et al., 2017). Porous geopolymer materials constitute viable alternatives for the treatment of industrial wastewater thanks to the ready availability of precursors in nature, their environmentally compatible

composition, and their nanoscale size/high volume pores and large specific surface area (Ge et al., 2015; Su et al., 2020). The advantage of use the geopolymers in adsorption process is theirs easily regeneration and their reuse after exhaustion in production of new building materials (Novais et al., 2020). Textile industry is one of the major industries using dyes to color their products; however, the waste solutions produced presents an environmental challenge of immense scale (Amjlef et al., 2021). Several techniques such as adsorption, photocatalytic degradation, precipitation, coagulation/flocculation, biodegradation, ion exchange and membrane separation have been used for decontaminating polluted wastewater (He et al., 2020; Ait El Fakir et al., 2021; Akhsassi et al., 2021; Bouddouch et al., 2021). More recently, porous geopolymers have been used for immobilization of radionuclides and radioactive waste generated from low-level waste stream (Kim et al., 2021; Niu et al., 2022). In general, adsorption methodologies are more widely preferred due to their efficiency, simplicity and low cost. Several works are devoted the adsorption of dye molecules from aqueous solution using the geopolymers materials, but their adsorption capacity doesn't reach those of others adsorbents materials such as soils, agricultural waste, unmodified and modified clay (Şahin et al., 2015). The advantage of geopolymers compared with raw clays and with others classical adsorbents is theirs high mechanic resistance, chemical and thermal stability allowed it her regeneration and recyclization (Novais et al., 2020).

The aim of this study is to develop a new eco-friendly and cost-effective porous geopolymer material based on a Moroccan natural pyrophyllite clay rich taken from Tata region. In order to promote the pore development in this geopolymer system a water:solid ratio of H_2O:Na_2O = 15 has been implemented, as described in previous work (Bouna et al., 2020). The geopolymers systems produced have been characterized by X-ray Diffraction (XRD), ^{29}Si and ^{27}Al magic-angle-spinning nuclear magnetic resonance (MAS NMR) analysis, Fourier Transform Infrared Spectroscopy (FTIR), Differential Thermal Analysis (DTA) and Thermal Gravimetric Analysis (TGA), N_2 adsorption/desorption isotherm analysis using the Brunauer-Emmett-Teller (BET) method and Scanning Electron Microscopy (SEM). In addition, the effectiveness of the newly synthesized porous geopolymers was gauged by measuring the stable uptake and elimination of methylene blue (MB) from aqueous solution. From an analysis of the adsorption mechanism process several kinetic and adsorption models such as Pseudo First Order (PFO), Pseudo Second Order (PSO), Intra Particles Diffusion (IPD), Langmuir, Freundlich and Temkin have been evaluated.

2. Materials and Methods

2.1. Materials

The raw pyrophyllite rich clay (PY) used in this work was acquired from the Addis village located in the Tata region of southern Morocco (29°41´31″N 7°58´25″W). This region belongs geologically in western part of Bani Mountain located in south of Anti-Atlas massif. The metal oxide composition of the raw (PY) sample was measured by X-ray Fluorescence analyses is presented in Table 1. Silicon dioxide, Sodium hydroxide and methylene blue chemicals compounds were purchased from Sigma-Aldrich, and they were used without further treatment.

Table 1: Chemical composition (wt.%) of the raw pyrophyllite rich clay (PY).

Oxides (wt.%)	**SiO_2**	**Al_2O_3**	**Fe_2O_3**	**K_2O**	**MgO**	**SO_3**	**CaO**	**Na_2O**	**P_2O_5**	**Loss on ignition**
PY	60.6	23.5	3.2	2.5	0.8	0.6	0.5	0.4	0.1	7.8

2.2. Porous Geopolymer Preparation

The natural raw pyrophyllite sample was coarsely crushed and ground, and sieved to a 50 µm particle size; this sample is denoted PY. PY-800 is the PY sample calcined at 800 °C for 8 h in air using a Lenton muffle furnace. PY-GPx (x = 1 - 7) are the geopolymers obtained after adding 2g of PY-800 to an alkaline activation solution previously prepared by the dissolution of desired amount of SiO_2 and NaOH in 15 ml of distilled water under vigorous magnetic stirring until it became a homogeneous gel (Table 2). The PY-GPx (x = 1 - 4) are the reaction mixtures stirred for 15 min for homogenization and then kept in oven at 70°C for 72 h for the geopolymerization reaction to proceed, whereas the PY-GPx (x= 5 - 7) samples are maintained at 25 °C. The solid recovered is crushed and washed successively with distilled water to remove the excess soluble unreacted matter (Fig. 1). The sample is recuperated by centrifugation, then dried and re-crushed for structural characterization and adsorption testing.

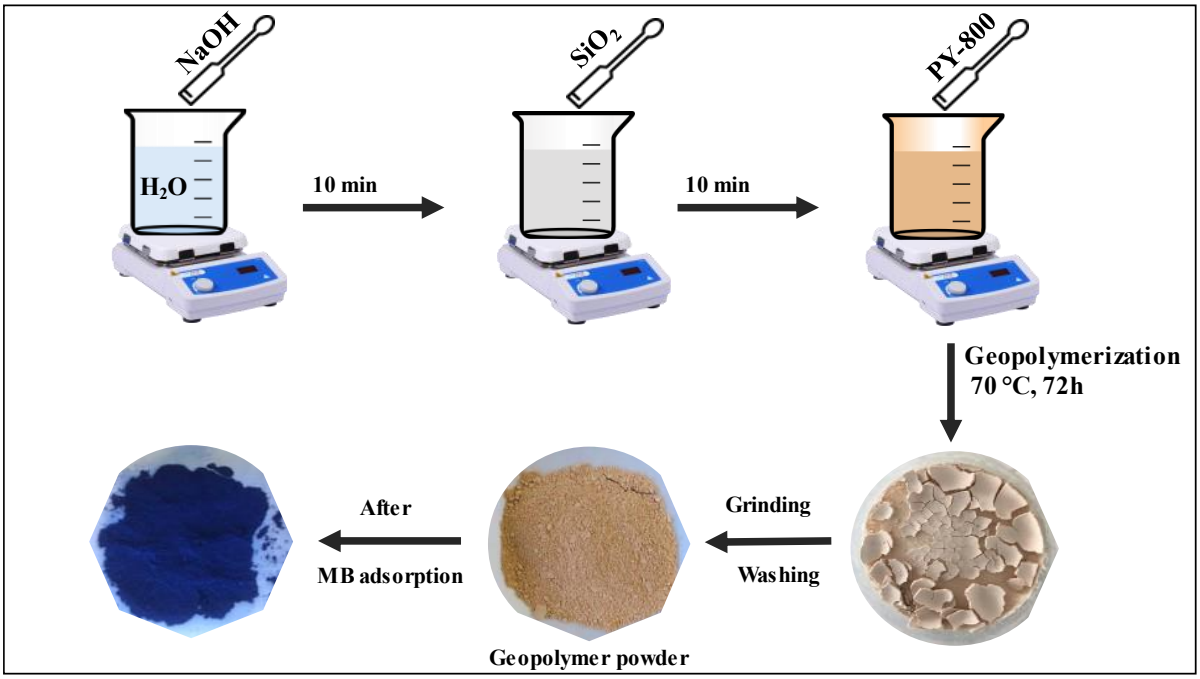

Fig. 1: Schematic representation of the porous PY-based geopolymer preparation.

Table 2: Synthesis conditions of each geopolymer preparation.

Geopolymer	PY-800 (g)	SiO_2 (g)	NaOH (g)	H_2O (ml)	Geopolymerization Temperature (°C)
PY-GP1	2	1	1	15	70
PY-GP2	2	0.5	1	15	70
PY-GP3	2	0	0.5	15	70
PY-GP4	2	0.5	0.5	15	70
PY-GP5	2	1	1	10	25
PY-GP6	2	0.5	1	10	25
PY-GP7	2	0.5	0.5	10	25

2.3. Characterization Methods

The chemical composition of raw natural pyrophyllite rich clay (PY) was determined by X-ray Fluorescence (Axios PANalytical spectrometer). The XRD data from the different geopolymer preparations were measured using a Bruker D8 Advance Twin diffractometer using KαCu irradiation at a wavelength of λ = 1.5418 Å. The diffraction patterns were determined over a 5 - 60° 2θ range, time of reckoning 0.3 s and step scanning of 0.05°. FTIR spectra were carried out in the range of 400 - 4000 cm^{-1} using the IRAffnity-1S Shimadzu spectrophotometer. TGA and DTA analyses were performed using the Q500 TA instrument. The TGA and DTA phenomena of raw PY and PY-GP4 samples were examined over a 25 -

1000 °C temperature range with a rate of 10 °C/min. The specific surface area of raw PY and PY-GP4 samples were determined using the BET method (Brunauer et al., 1938), while the N_2 adsorption/desorption isotherms at 77 K were utilized using a 3FLEX (Micromeritics, USA) analyzer type. The total pore volume V_T was determined from the volume of N_2 gas adsorbed at relative pressure of 0.89, with each sample being outgassed at 200 °C for 12 h prior to measurement. SEM analysis was used to examine the morphology of each geopolymer preparation; this was undertaken using a Jeol TSM-IT100 operating at a voltage of 20 KeV, coupled with an Energy Dispersive X-rays Spectroscopy (EDS) analyzer.

All ^{29}Si measurements were performed at 7.05 T using a 300 MHz Bruker Avance III HD spectrometer operating at ^{29}Si Larmor frequency (ν_o) of 59.63 MHz. These experiments were performed using a Bruker 7 mm HX probe which enabled a MAS frequency of 5 kHz to be implemented. The pulse length calibration was performed on solid kaolinite ($Al_2Si_2O_5(OH)_4$) from which a $\pi/2$ pulse time of 6 μs was determined. Quantitative single pulse measurements were undertaken using a recycle delay of 240 s. The reported ^{29}Si chemical shifts were externally referenced against the primary reference of $(CH_3)_4Si$ (1% in $CDCl_3$, δ_{iso} = 0.0 ppm) via the secondary solid kaolinite reference (δ_{iso} = –91.5 ppm) (Watanabe et al., 1987; Harris et al., 2002). The corresponding 1D ^{27}Al MAS NMR study was undertaken at 9.4 T and 11.7 T using Bruker Avance 400 MHz and Bruker Avance 500 MHz spectrometers, respectively. These experiments were performed using Bruker 3.2 mm HX probes which enabled a MAS frequency of 20 kHz throughout. The ^{27}Al pulse length calibration was performed on a 1.1 M $Al(NO_3)_3$ solution where a non-selective (solution) $\pi/2$ pulse length of 9 μs was determined, thus equating to a selective (solid) $\pi/2$ pulse length of 3 μs for the I = 5/2 ^{27}Al nucleus. Semi-quantitative data was acquired using single pulse experiments employing a $\pi/6$ pulse length of 1 μs and a recycle delay of 30 s. The reported centre-of-gravity (apparent) shifts (δ) and isotropic (δ_{iso}) ^{27}Al chemical shifts were externally referenced against the primary 1.1 M $Al(NO_3)_3$ solution reference (in D_2O, δ_{iso} = 0.0 ppm) (Harris et al., 2002). The spectral simulation of all ^{29}Si and ^{27}Al MAS NMR data was performed using the DMfit software package (Massiot et al., 2002). Additional 2D ^{27}Al MQMAS data were acquired using a three-pulse z-filtered pulse experiment. Typical pulse widths for the excitation, conversion and soft z-filter pulses were 2.4, 0.8, and 9.8 µs, respectively. In similar fashion to the 1D MAS NMR data, the ^{27}Al chemical shift referencing was undertaken externally against the primary reference of $Al(NO_3)_{3(aq)}$ (1.1 mol in D_2O, δ_{iso} = 0.0 ppm) (Harris et al., 2002).

2.4. Adsorption Tests

For the present study, methylene blue (MB) was chosen as the organic pollutant model dye due to its potential relevance to the textile industry, and the ease of incorporation and manipulation in the experimental testing. We have studied a several indicators that influence the MB adsorption phenomena including adsorbent mass, pH, contact time, MB initial concentration and temperature effect. These adsorption conditions are given in Table 3.

Table 3: Methylene blue adsorption tests conditions

Parameters studied	Temperature (°C)	pH	Geopolymer powder mass (mg)	Contact time (min)	MB initial concentration (mg/L)	MB solution volume (mL)
adsorbent mass effect	25	7	20-200	180	100	25
pH effect	25	2-10	60	180	100	25
Stirring time effect	25	7	60	5-240	100	25
MB Initial concentration effect	25	7	60	120	50-300	25
Temperature effect	25 35 45 55	7	60	120	100	25

The pH values are adjusted with 0.1M HCl and 0.1M NaOH solutions and are monitored using a pH meter. The adsorption experiments are arranged in batch conditions into a beaker under vigorous stirring to keep liquid/solid ratio constant. Aliquots of 3ml volume were removed after a contact time period, then separated by centrifuge at 4000 rpm for 2 min and analyzed with a 6705 UV/Vis spectrophotometer operating at a wavelength of 664 nm.

The adsorption capacity at equilibrium (q_e), the adsorption capacity any time t (q_t) and the percentage of MB removed at any time t are determined by equations (1), (2) and (3), respectively (Suopaja et al., 2020; Amjlef et al., 2021) :

$$q_e = \frac{(C_i - C_e)}{\mathrm{m}} V \qquad (1)$$

$$q_t = \frac{(C_i - C_t)}{m} V \qquad (2)$$

$$\%\, Removal = \frac{(C_i - C_t)}{C_i} 100 \qquad (3)$$

In these equations C_i, C_e and C_t are the initial concentration, equilibrium concentration and concentration at time t of MB concentration in mg/L, respectively, while V is the volume of solution (in L) and m is the mass of adsorbent (in g).

3. Results and Discussion

3.1 XRD Analyses

The X-ray diffraction data of the raw PY clay, PY-800 calcined phase and different geopolymers elaborate PY-GPx (x = 1 - 7) are shown in Fig. 2. The diffractogram of the raw PY sample exhibits intense characteristic reflections from pyrophyllite ($Al_2Si_4O_{10}(OH)_2$, JCPDS: 96-900-0277), muscovite ($KAl_2(AlSi_3O_{10})(OH)_2$, JCPDS: 96-900-4642), kaolinite ($Al_2Si_2O_5(OH)_4$, JCPDS: 80-0886) and quartz (SiO_2, JCPDS: 96-900-9667). Corresponding diffraction data from the calcined PY-800 fraction shows the disappearance of the kaolinite reflections which exhibits reduced crystallinity under thermal treatment due to structural disorder induced by high temperature dehydroxylation of this system (Bouna et al., 2020; Sayed et al., 2020). The reflections from the quartz and pyrophyllite components are unchanged except for the characteristic (003) reflection of pyrophyllite appearing at 29.08° (2θ) which moves to a smaller angle 28.7° (2θ) that due to the PY dehydroxylation after calcination at 800 °C (Li et al., 2014; Erdemoğlu et al., 2020). In contrast, the muscovite was transformed to potassium aluminum silicate phase ($K(Si_3Al)(Al_2)O_{11}$, JCPDS: 046-0741) (Bouna et al., 2020) upon calcination. For the synthesized geopolymer samples PY-GPx (x = 1 - 7) the appearance of the amorphous hump in 20 - 35° 2θ angular range is observed to be more intense in the PY-GP1, PY-GP4 and PY-GP5 samples which are geopolymer syntheses at both 70°C and at room temperature, thus suggesting that the observed amorphous component is independent of geopolymerization temperature. All geopolymers spectra shown the very intense reflections of both pyrophyllite and potassium aluminum silicate phases indicate theirs low chemical activation. In the next study, we have choosing PY-GP4 sample for undergo more characterization method and realize the adsorption tests. The last is geopolymer elaborate with lower chemical activators (Table 2) and prepared quickly because those prepared at room temperature demand more days for drying.

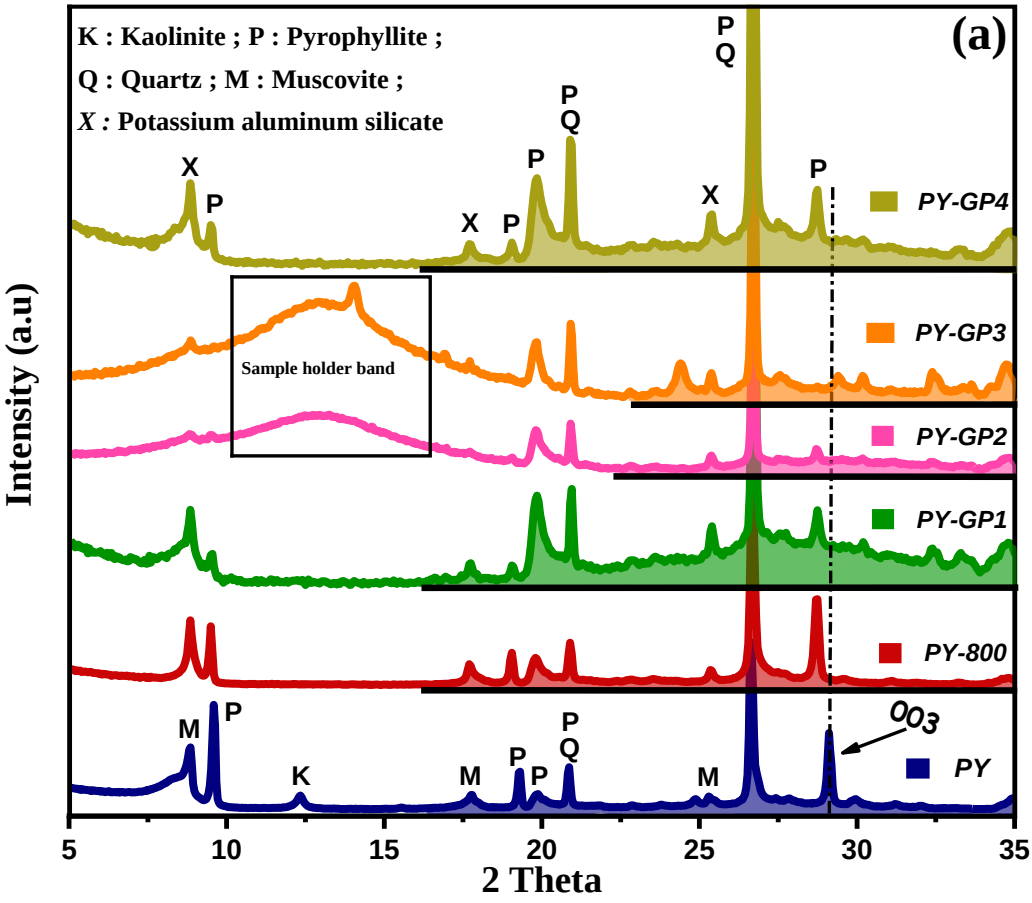
K : Kaolinite ; P : Pyrophyllite ;
Q : Quartz ; M : Muscovite ;
X : Potassium aluminum silicate
(a)
Sample holder band
PY-GP4
PY-GP3
PY-GP2
PY-GP1
PY-800
PY
003
Intensity (a.u)
2 Theta

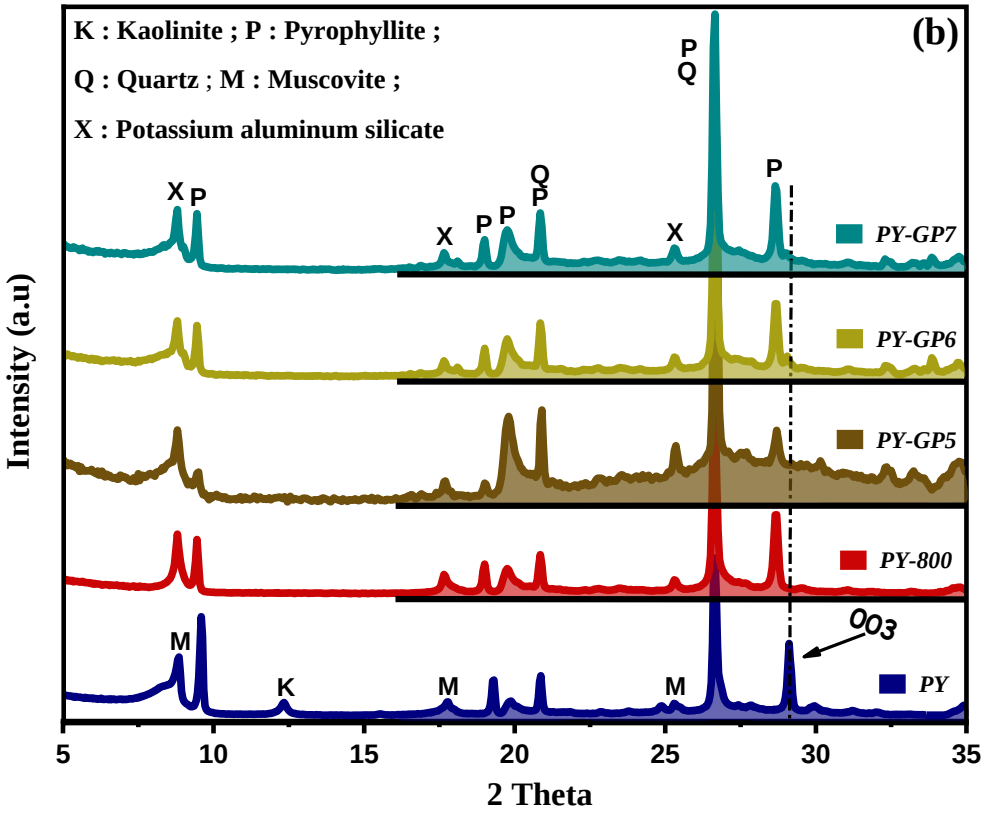
K : Kaolinite ; P : Pyrophyllite ;
Q : Quartz ; M : Muscovite ;
X : Potassium aluminum silicate
(b)
PY-GP7
PY-GP6
PY-GP5
PY-800
PY
003
Intensity (a.u)
2 Theta

Fig. 2: XRD data from the PY raw clay, PY-800 calcined fraction and geopolymers samples PY-GPx (x = 1, 2, 3 and 4) geopolymers prepared at (a) 70°C, and (b) PY-GPx (x = 5, 6 and 7) geopolymers prepared at room temperature.

3.2 ^{29}Si and ^{27}Al Magic Angle Spinning Nuclear Magnetic Resonance (MAS NMR) Analyses

The experimental and deconvoluted ^{29}Si and ^{27}Al MAS NMR data from the PY raw clay, PY-800 calcined fraction and PY-GP4 prepared geopolymer samples are presented in Figs. 3(a) - (c), with the chemical shifts and the quadrupole coupling constants reported in Tables 4 and 5. For the PY raw sample, the prominent resonance at ~–96 ppm Q^4(1Al) is attributed to a pyrophyllite clay phase (Fitzgerald et al., 1996; Li et al., 2014), while the signals at ~–108 and ~–112 ppm correspond to the fully condensed Q^4(0Al) Si species of quartz and amorphous silica, respectively, which are present in the raw sample (Mackenzie and Smith, 2002). The quartz assignment is corroborated by the XRD analysis above. The ^{29}Si broad resonances in the –80 - –95 ppm range are contributions from Q^3(0Al) (~–93 ppm), Q^3(1Al) and Q^3(2Al) species; the former resonance is the well-characterised hydroxylated Q^3(0Al) Si position in kaolinite (Mackenzie and Smith, 2002), while the latter observed at ~–86 ppm represents Q^3(1Al) and Q^3(2Al) species associated with a muscovite phase present in the raw material (Weiss et al., 1987). Only two resonances are observed in the variable field ^{27}Al MAS NMR data in Figs. 3(b) and (c); these correspond to four coordinate AlO_4 positions in the muscovite phase and six coordinate AlO_6 positions associated with the kaolinite, muscovite and pyrophyllite phases (Sanz and Serratosa, 1984). The broad ^{29}Si linewidths observed for these Q^3 resonances, together with the extended tailing of the ^{27}Al AlO_4 and (in particular) AlO_6 resonances on the high field/low ppm side suggests that significant structural disorder is associated with all three phases.

Upon calcination of the pyrophyllite phase at 800 C, the ^{29}Si and ^{27}Al MAS NMR data from the PY-800 sample exhibits clear evidence of dehydroxylation under this thermal treatment. The ^{29}Si resonance at ~–96 ppm shifts to ~–102 ppm (see Fig. 3(a)) (Sainchez-soto et al., 1993), while the Al speciation exhibited in Figs. 3(b) and (c) assumes greater complexity. Of particular note is the second order broadened five coordinate (AlO_5) pyrophyllite resonance at δ_{iso} ~25 ppm (C_Q = 10.5 MHz, η_Q = 0.0) resulting from the $AlO_5(OH) \rightarrow AlO_5$ dehydroxylation process. This observation is consistent with previous studies (Sainchez-soto et al., 1993; Sa´nchez-Soto and Pe´rez-Rodrı´guez, 1997). Upon the loss of the OH^- group the Al speciation transforms from six coordinate to five coordinate thus reducing the point symmetry and markedly

increasing the linewidth, although axial point symmetry (η_Q = 0.0) is maintained. The accuracy of the deconvoluted ^{27}Al MAS NMR data is confirmed by constraining these field dependent data at different external magnetic field strengths, as evidenced in Figs. 3(b) and (c) and Table 5. The thermal transformation process also induces an increase in AlO_4 speciation at the expense of AlO_6 inventory from the clay compositions, with an additional AlO_5 transitional species (δ_{iso} ~25 ppm) also being observed; however, this AlO_5 species is characterized by a significantly narrower linewidth and smaller quadrupolar parameters in comparison to the AlO_5 species generated by the pyrophyllite dehydroxylation process (C_Q ~10.5 MHz vs. 3.1 MHz) (Bradley and Hanna, 1993, 1994; Samuel et al., 2021).

For the final PY-GP4 geopolymer preparation the ^{29}Si MAS NMR data of Fig. 3(a) shows that most of the Si speciation is dominated by shifts in the –80 - –95ppm range. These structural moieties are condensed Q^4 Si units with a predominance of Al in the next-nearest-neighbor coordination sphere (Rowles et al., 2007; Tsai et al., 2010; Walkley et al., 2018; Tian et al., 2020). Structural units such as Q^4(2Al), Q^4(3Al) and Q^4(4Al) are intrinsic to the amorphous geopolymer network and form selectively at the expense of AlO_5 and AlO_6 speciation (Rowles et al., 2007; Walkley et al., 2018; Samuel et al., 2021). In additional to the ^{29}Si MAS NMR characterisation, the ^{27}Al MAS NMR data of Figs. 3(b) and (c) demonstrate the predeominance of AlO_4 moieties defining this network, although these data also show that some residual/unreacted muscovite and pyrophyllite clay components still exist in the system. The ^{27}Al MQMAS data in Figs.3 (d)-(f) also confirms that the disordered muscovite phase is persistent thoroughout the geolpymer transformation process. These data also demonstrate that the short range disorder affecting the AlO_4 and AlO_6 positions has different origins, with the AlO_4 species being influenced by chemical shift dispersion while the AlO_6 species are dominated by distributions of quadrupolar parameters introduced by disorder in the Al-O bond lengths and bond distances (Rowles et al., 2007; Walkley et al., 2018).

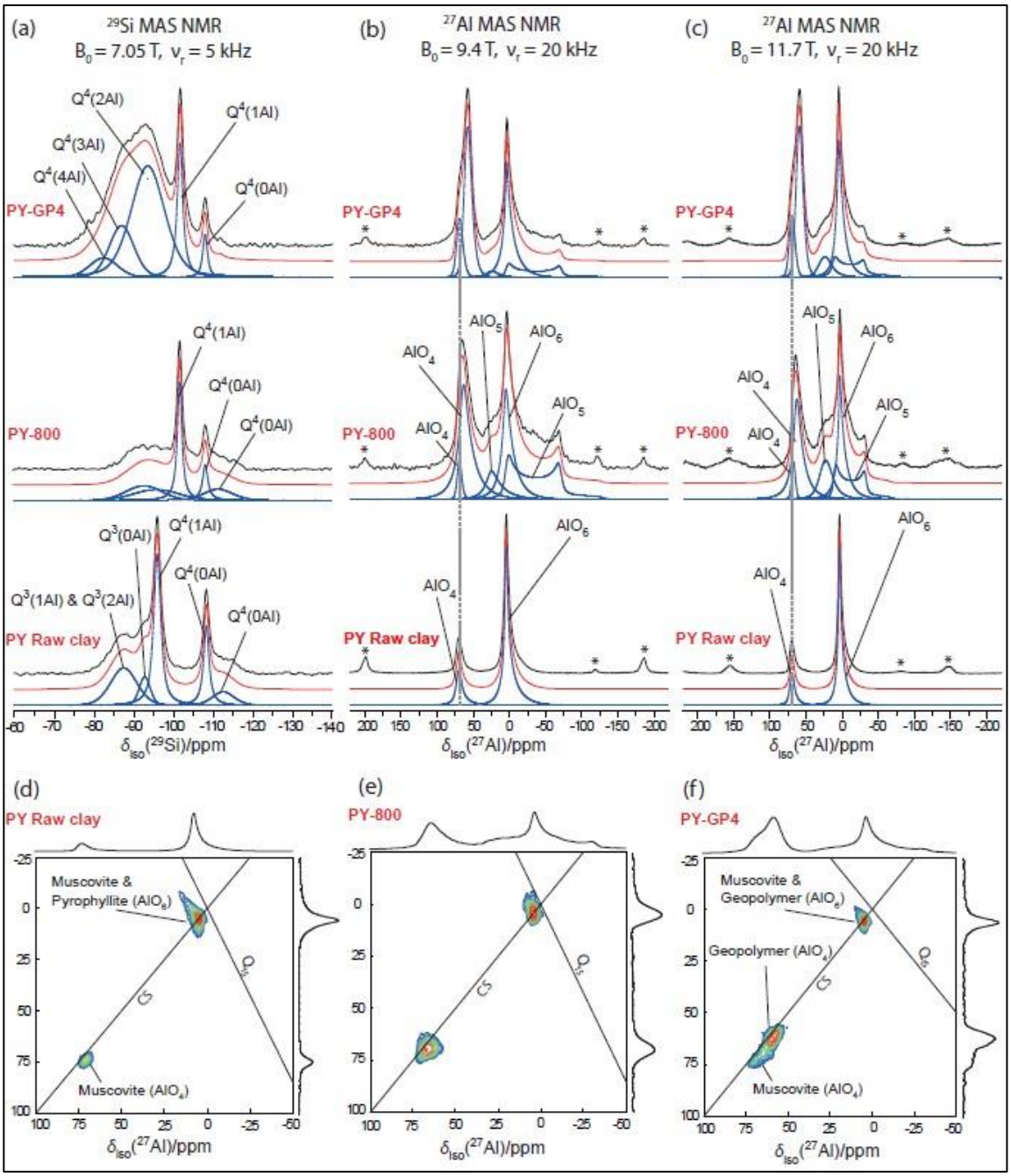

Fig. 3: Solid state NMR study showing the (a) ^{29}Si MAS NMR data, (b), (c) variable field ^{27}Al MAS NMR data, and (d)-(f) ^{27}Al MQMAS data from the PY raw clay, PY-800 calcined fraction and PY-GP4 prepared geopolymer systems. The resonances marked with asterisks (*) represent spinning sidebands.

Table 4: The assignment of the chemical shifts from the ^{29}Si MAS NMR data.

Assignment	δ_{iso} (^{29}Si)/ppm (± 1)
Q^4(0Al) Silica (amorphous)	–112
Q^4(0Al) Quartz	–108
Q^4(1Al) Pyrophyllite (dehydroxylate)	–102
Q^4(1Al) Pyrophyllite (hydroxylate)	–96
Q^4(2Al)	–93
Q^4(3Al)	–87
Q^4(4Al)	–82

Table 5: The assignment of the chemical shifts from the ^{27}Al MAS NMR data.

Assignment	δ_{iso} (^{27}Al)/ppm (± 2)	C_Q/MHz (± 0.05)
Muscovite (AlO_4)	72	2.4
Muscovite & Pyrophyllite (AlO_6)	8	3.4
Pyrophyllite Dehydroxylate	25	10.5 (η_Q = 0.0)
Geopolymer (AlO_4)	61	2.3
Geopolymer (AlO_5)	25	3.1
Geopolymer (AlO_6)	5	2.6

3.3 Infrared Spectroscopy Analyzes

Fig. 4 shows the FTIR spectra of the raw PY clay, the calcined PY-800 fraction and the prepared PY-GP4 geopolymer. The bands at 562 and 474 cm^{-1} present in each sample are ascribed to characteristic deformation vibrations of the Si-O bond previously reported in clay minerals (Li et al., 2014), while the band observed at 798 cm^{-1} is attributed to quartz Si-O bond vibrations (Bouna et al., 2020). Intense bands in the 1029 - 1047 cm^{-1} range are characteristic of asymmetric stretches in Si-O bonds, with the shifting position from 1047 cm^{-1} (for the calcined PY-800 precursor) to 1029 cm^{-1} (for geopolymer PY-GP4) suggests successful activation of meta-pyrophyllite phase with the alkaline activation solution and formation of geopolymer matrix (Singhal et al., 2017; Hu et al., 2020). The moderately intense band at 3650 cm^{-1} appearing in the raw PY spectrum is characteristic the of OH vibrations associated with pyrophyllite, muscovite and kaolinite clays; this band disappears from PY-800 sample under calcination (dehydroxylation) conditions at 800 °C (Li et al., 2014; Wan et al., 2017). A less intense band appearing at 1649 cm^{-1} is assigned to bending deformation modes of adsorbed water (Singhal et al, 2017; Tchakouté et al., 2021). This band is more prominent in the geopolymer PY-GP4 sample. A large band distributed over the 2800-3750 cm^{-1} range is associated with the PY-GP4 data is characteristic of OH vibrations observed in amorphous

geopolymers (Bouna et al., 2020). For PY-GP4@MB; the sample obtained after methylene blue adsorption. We show the appearance of news vibrations bands at 1342, 1387, 1503 and 1607 cm^{-1} attributable to the bending vibrations of methylene blue molecule adsorbed into geopolymer surface (Dzoujo et al., 2022). Furthermore, we observed the narrowing of the band characteristic of OH vibrations (2800-3750 cm^{-1}) that confirm and highlight the MB molecules fixation (Dzoujo et al., 2022).

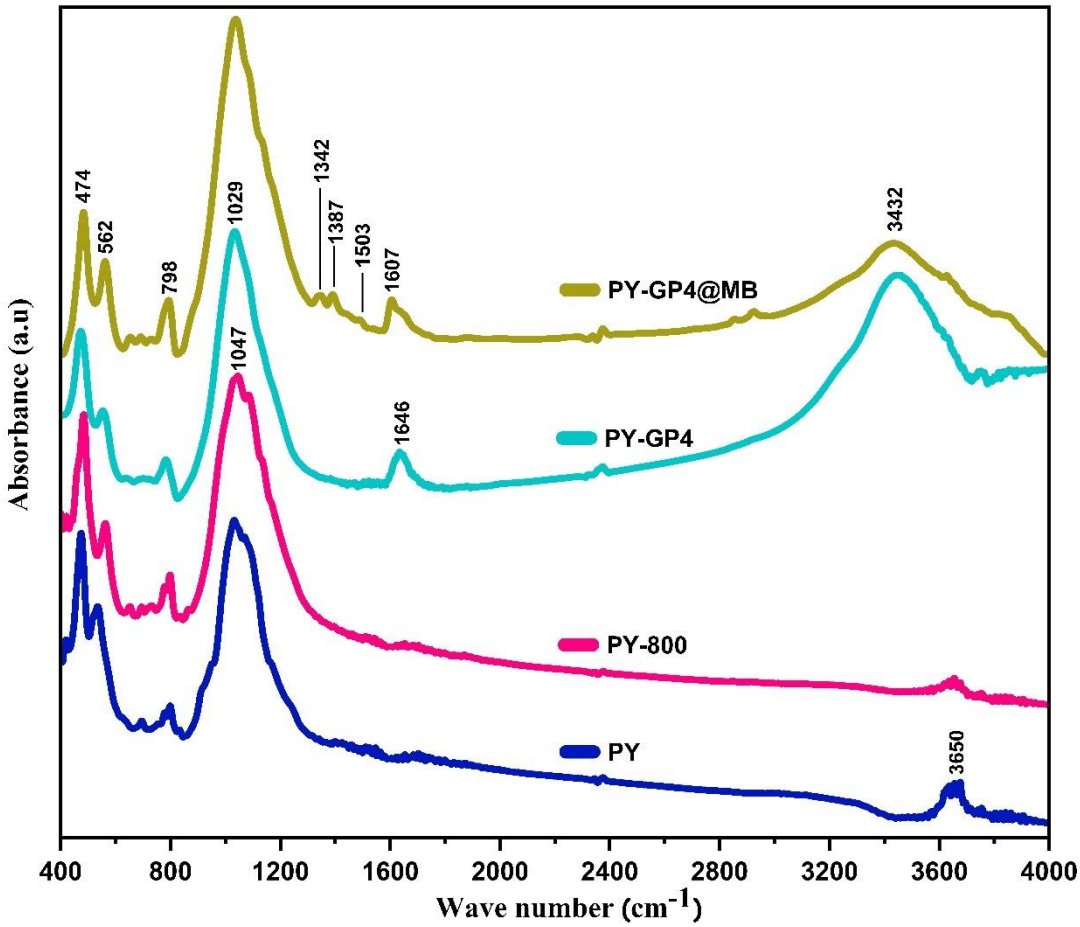

Fig. 4: FTIR spectra of the raw PY clay, the calcined PY-800 fraction, the synthesized geopolymer PY-GP4 and PY-GP4@MB sample obtained after MB molecules adsorption.

3.4 TGA/DTA analysis

Fig. 5 present the thermograms and differential thermal analysis data for the raw PY clay and the synthesized PY-GP4 geopolymer as a function the heating temperature. The data from the raw PY clay shows the presence of two endothermic transitions. The first (observed over the 50-110 °C range) is associated with a mass loss of 2.2% and corresponds to the removal of physisorbed water from the particle surfaces and pore structure of the clay minerals (Pérez-

Maqueda et al., 2004), while the second endothermic transition (appearing over the 420-915 °C range) associated with a mass loss of 5.5% is attributed to dehydroxylation of the pyrophyllite, kaolinite and muscovite clays minerals present in raw sample (Guanghui et al., 2014; Erdemoğlu et al., 2020). The prepared PY-GP4 geopolymer shows a significant increase in mass loss of physisorbed water (4.7%) compared to raw PY sample confirming the development of important attributes such porosity and permeability resulting from the geopolymer synthesis conditions (Bouna et al., 2020). In addition, the very low mass loss observed above 400°C (~0.4%) from the PY-GP4 geopolymer indicates a highly stable system resulting from the use of PY-800 (metapyrophyllite) precursor phase used for the geopolymer formation.

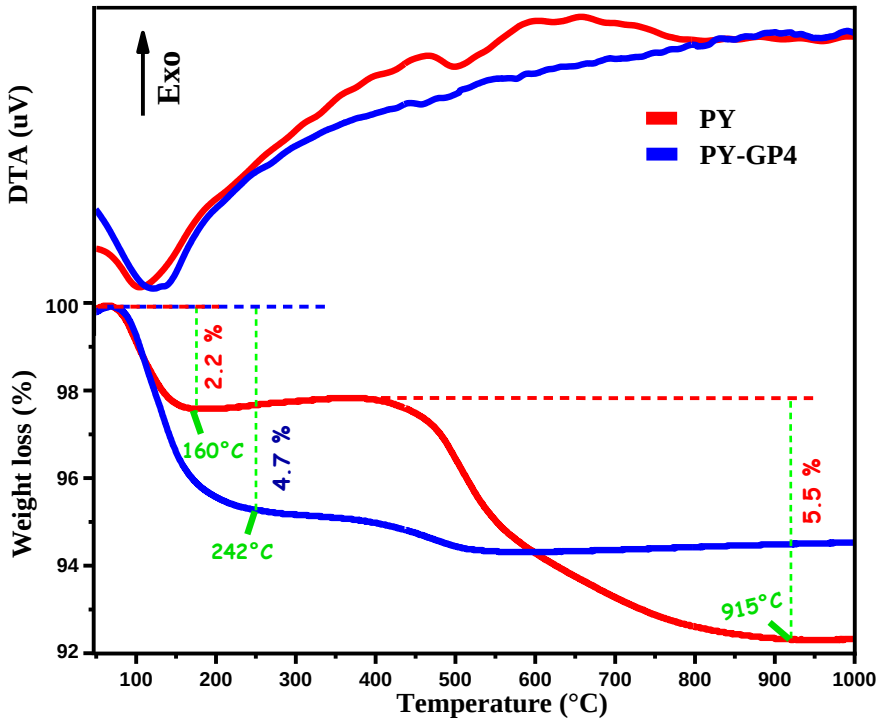

Fig. 5: TGA/DTA curves of PY raw sample and PY-GP4 prepared geopolymer.

3.5 BET Surface Area Assessment

The adsorption-desorption isotherm curves from the raw PY clay and the prepared PY-GP4 geopolymer are presented in **Fig. 6**. Both data sets demonstrate type IV isotherms with H3 hysteresis loops in accordance with International Union of Pure and Applied Chemistry (IUPAC) classifications, indicating that the geopolymer nanostructure is comprised of slit-like shaped pores. As previously reported, this isotherm and hysteresis behaviour is characteristic of mesoporous materials (Sing et al., 1985; Bouna et al., 2020). For the PY-GP4 geopolymer, both specific surface area (S_{BET} = 86.5 m^2/g) and pore volume (Vp = 0.08 cm^3/g) have

significantly increased in comparison to the raw PY raw clay (S_{BET} = 30.0 m^2/g, Vp = 0.05 cm^3/g (see Table 6). This result indicates that the implemented geopolymerization process increases the specific surface area and stimulates the development of new micro and mesoporous sites in the final material (see Table 6). Similar isotherm and hysteresis types have been recently reported by Singhal *et al*. and Bouna *et al*. (Singhal et al., 2017; Bouna et al., 2020)**.**

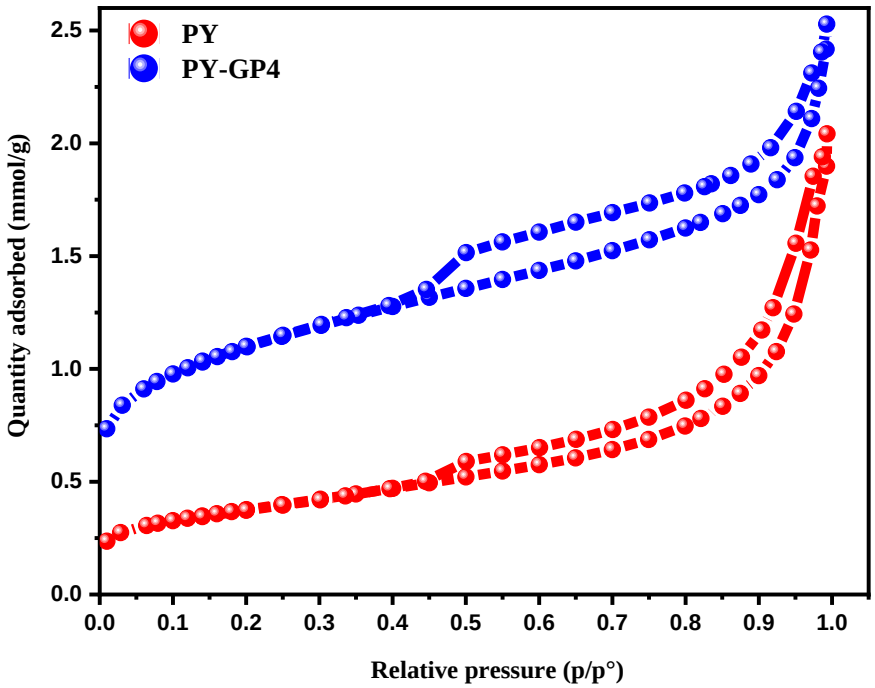

Fig. 6: Nitrogen adsorption-desorption isotherms from the raw PY clay and the synthesized PY-GP4 geopolymer sample.

Table 6: Specific surface area S_{BET}, microporous V_{mic}, mesoporous V_{mes} and total of pore volume V_T values of PY raw clay and PY-GP4 prepared geopolymer sample.

	S_{BET} (m^2/g)	V_{mic} (cm^3/g)	V_{mes} (cm^3/g)	V_T (cm^3/g)
Raw PY sample	30.00±0.1	-	0.053	0.053
PY-GP4 geopolymer	86.58±0.6	0.012	0.074	0.086

3.6 SEM Analysis

The sample morphology observed from powdered samples of the raw PY clay, the calcined PY-800 fraction, prepared PY-GP4 geopolymer and PY-GP4@MB sample obtained after MB dye adsorption as observed by SEM micrographs are presented in Fig. 7. Table 7 shows the EDS analyses of various samples, the high atomic percentages obtained for Si and Al elements

confirms the aluminosilicate character of our materials. The images presented in Figs 7a and 7b exhibit morphologies characteristic of pyrophyllite clay mineral (Erdemoğlu et al., 2004; Zhang et al., 2015; El Gaidoumi et al., 2019, 2019) ; however, 7c and 7d images shows an altered morphology associated with the calcined PY-GP4 phase pyrophyllite. Moreover, 7e and 7f images present the morphologies that are aligned with amorphous and porous geopolymers systems (Bouna et al., 2020). From these images heterogeneous and disordered microstructures with the presence of the inter-particle pores can be observed for the geopolymer PY-GP4 in comparison to the raw PY clay and calcined PY-800 fraction. This morphology corroborates the results highlighted by the FTIR, TGA/DTA and BET analysis methods reported above, and agrees with previously reported findings from other studies (Bouna et al., 2020; Lertcumfu et al., 2020). For PY-GP4@MB; sample obtained after MB molecules adsorption, 7g and 7h image shows a more homogeneous surface and a lower porosity compared to those of the starting material (PY-GP4). In addition, the EDS analysis of the PY-GP4@MB sample (**Table 7**) detects the C and S elements correspond to the MB molecules fixed on the surface and the pores of our geopolymer material.

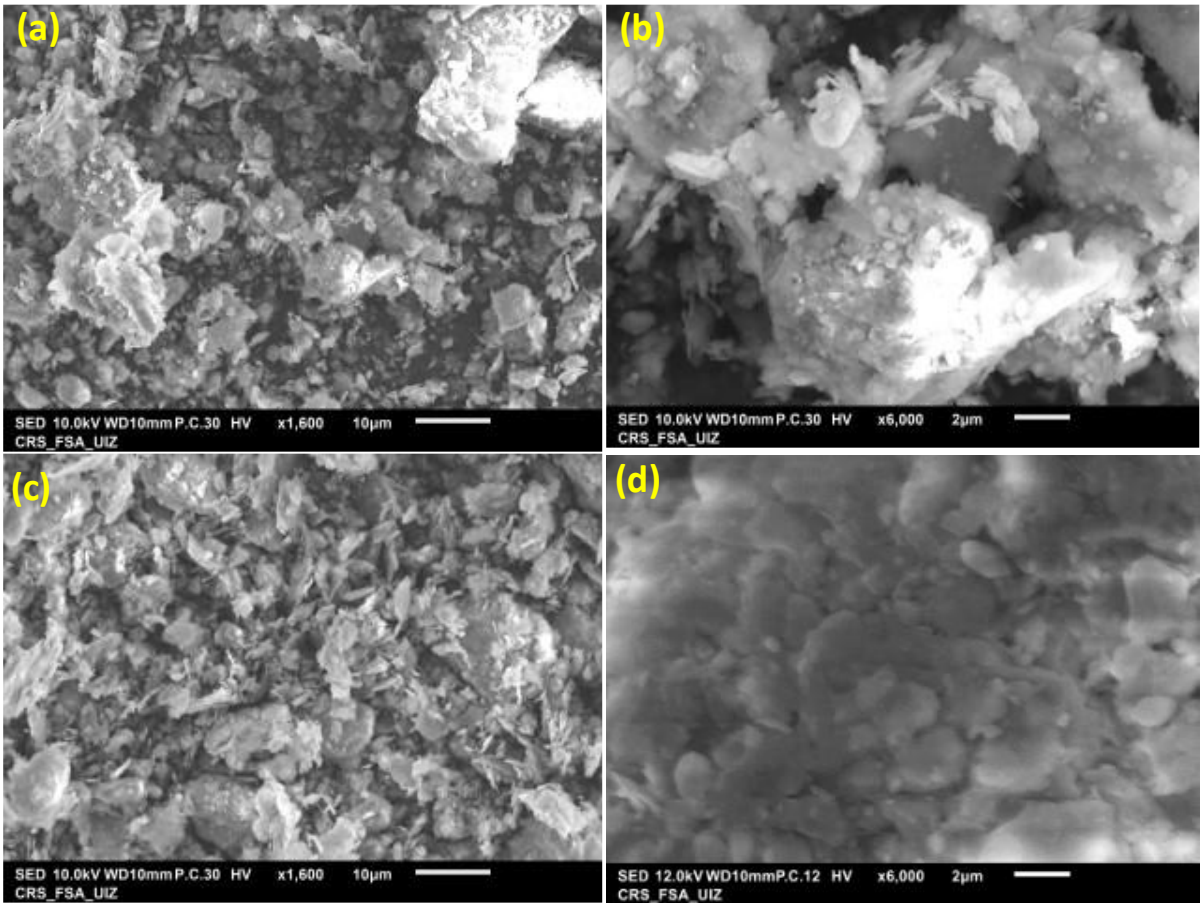

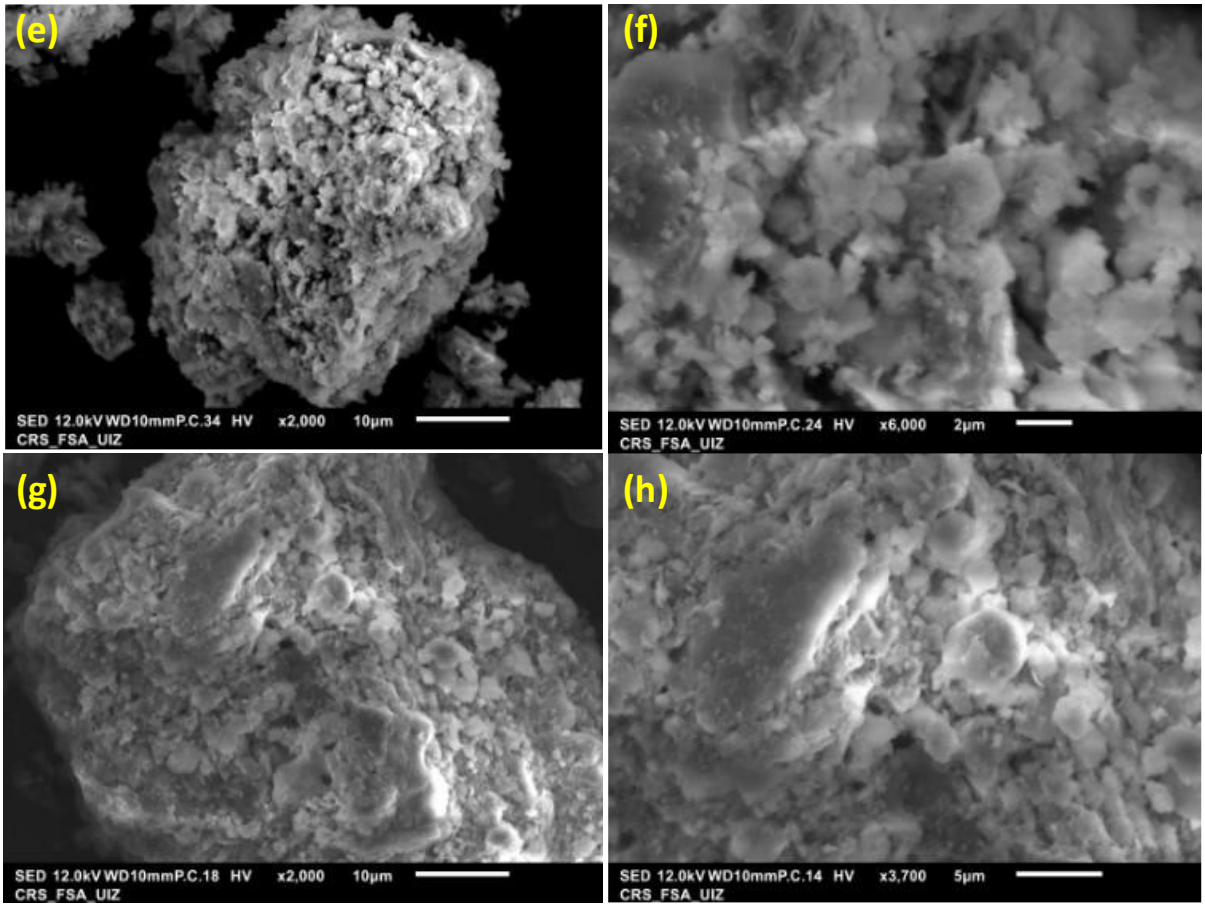

Fig. 7: SEM micrographs of, (a, b) raw PY clay, (c, d) calcined PY-800 fraction, (e, f) prepared PY-GP4 geopolymer and (g,h) sample PY-GP4@MB obtained after MB fixation.

Table 7: EDS atomic percentage of, raw PY clay, calcined PY-800 fraction, prepared PY-GP4 geopolymer and PY-GP4@MB: sample obtained after methylene blue adsorption.

	% Atomic							
	Si	**Al**	**K**	**Na**	**Mg**	**Ti**	**C**	**S**
PY	62.41	27.85	5.74	1.63	1.23	1.14	-	-
PY-800	62.19	29.50	6.82	1.48	-	-	-	-
PY-GP4	64.43	27.28	6.71	1.57	-	-	-	-
PY-GP4@MB	47.62	24.52	3.25	2.12	1.20	-	20.92	0.34

4. Adsorption Tests

4.1 Parameters Affecting the Adsorption Experiments

The effect of adsorbent mass, stirring time and pH are presented in Figs. 8a, b, and c, respectively. All experiments were realized in batch condition at room temperature under magnetic stirring. Fig. 8a shows the amount adsorbed of methylene blue dye MB present in aqueous solution on different mass of our prepared geopolymer powder PY-GP4. The mass of adsorbent effect was studied in 0.8 - 8 g/L range, the initial MB concentration was fixed at 100 mg/g, the delay of stirring is 2h and all experiments were stabilized at pH = 7. The curve obtained shows that between 0.8 - 2.4 g/L interval the removal amount of MB increases with increasing of adsorbent mass indicating the presence of adsorption-active sites in the geopolymer PY-GP4 system (Ge et al., 2017). Then, we obtained a pallier from 2.4 - 8 g/L indicate the total adsorption of MB molecules into porous geopolymer adsorbent. We have chosen the adsorbent concentration 2.4 g/L for realize the next study.
Fig. 8b shows the adsorbed amount of MB over time. This experiment was realized in the following conditions; [adsorbent] = 2.4 g/L g/L, $[MB]_0$ = 100 ppm and pH = 7. These results show that the adsorption amount increases with increasing of the contact time until saturation of 90 min is reached. Therefore, the equilibrium time selected in all subsequent studies is 120 min.

The influence of pH medium was studied in 2 - 10 interval, the adsorbent concentration was fixed at 2.4 g/L, $[MB]_0$ = 100 mg/L, stirring time was 2 h. The obtained results presented in Fig. 8c indicate that the amount of MB adsorbed on PY-GP4 surfaces increases with increasing of the pH value. This result can be explained by the creation of new adsorption sites due to an increase of negative charge density on the pore surfaces induced by deprotonation of M-OH species under the influence of OH^- entities present in basic medium according to the following reaction (4) (Su et al., 2020):

$$\mathbf{M\text{-}OH + OH^- \rightarrow M\text{-}O^- + H_2O\ (M= Si\ ou\ Al)} \qquad \mathbf{(4)}$$

Therefore, the large amount of MB adsorbed in basic medium is mainly induced by electrostatic forces due to the attraction between the cationic MB dye and the negative surface charge of the pores within the adsorbent material (Bouna et al., 2020; Hermann et al., 2021). For our sample, the contribution of MB adsorbed favored by the basic medium compared with acidic medium was about 2%. This low involvement is in high agreement with the thermal analyses results which show that the loss mass of (OH) entities appearing over the 420-915 °C range in our elaborate geopolymer sample was only 0.4% (**Fig. 5**).

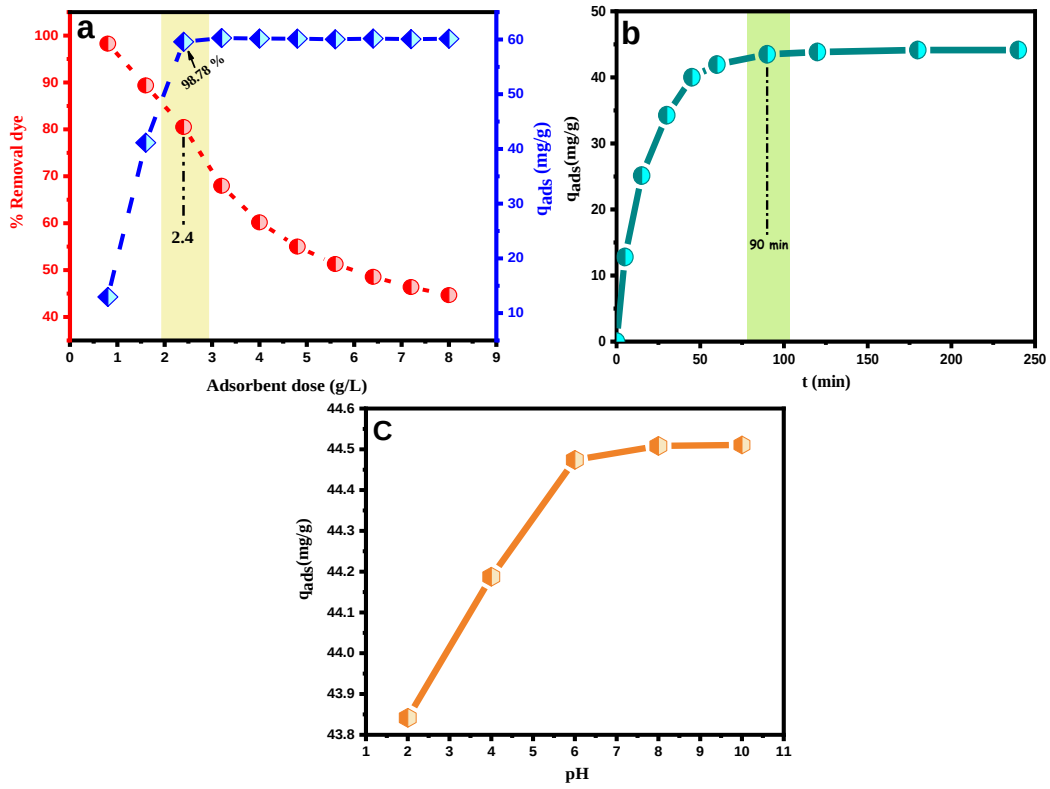

Fig. 8: Parameters affecting the adsorption experiments: (a) adsorbent mass, (b) stirring time and (c) pH of medium.

4.2 Adsorption Kinetics

The adsorption kinetics have been provided to understand the adsorption mechanism between the adsorbate and adsorbent. In this present work, three kinetics models have been described for following the adsorption kinetics of MB cationic dye uptakes by our new porous geopolymer elaborate based on the natural PY clay, namely PFO, PSO and IPD as described above in equations (1), (2) and (3), respectively. The linear form of these models are presented in equations 5, 6 and 7, respectively. Table 8 summarizes the characteristics parameters calculated for the three kinetics models.

$$Log\,(q_e - q_t) = Log\,q_e - \frac{K_1}{2.303}t \qquad (5)$$

$$\frac{t}{q_t} = \frac{1}{K_2 q_e^2} + \frac{1}{q_e}t \qquad (6)$$

$$q_t = K_{int}t^{0.5} + C \qquad (7)$$

where q_e and q_t are adsorbed amounts at equilibrium and time t in $mg.g^{-1}$, respectively. k_1 (min^{-1}), k_2 ($g.mg^{-1}.min^{-1}$) and k_{int} are the first order rate constant, second order rate constant and intra-particle diffusion constant, respectively.

After comparing the various parameters obtained in Table 8, it is concluded that the PSO model is the most acceptable compared to the PFO and IPD models. This conclusion is further supported by the linear correlation coefficient found which is very close to a value of 1, as well as the adsorbed amount of MB at equilibrium (q_e) is calculated by the PSO model to be very close to the experimental value q_e^{exp} = 43.5 mg/g.

Table 8: Parameters kinetics determined from PFO, PSO and IPD models obtained for the MB adsorption on porous geopolymer adsorbent.

Models	Parameters	
Pseudo first order	R^2	0.987
	K_1 (min^{-1})	0.008
	q_e (mg/g)	32.359
	q_e^{exp} (mg/g)	43.45
Pseudo second order	R^2	0.998
	K_2 (g/mg.min)	0.002
	q_e (mg/g)	49.50
	q_e^{exp} (mg/g)	43.45
Intra particle diffusion	R^2	0.9612
	K_{int} ($g.\ mg^{-1}.min^{-1/2}$)	0.073
	C (mg/g)	2.848

4.3 Adsorption Model

a- Initial dye Concentration Effect

Fig. 9 shows the evolution of MB adsorbed amount on the porous geopolymer adsorbent as function of dye initial concentration. The measured uptake shows behavioral regions; in the first stage spanning the 50 - 200 mg/g range an increase of adsorbed MB with increasing of initial concentration is observed that indicates the existence of vacant actives sites on adsorbent surface. Beyond 200 mg/g an invariant plateau is established indicating saturation of the active adsorption sites. The maximum amount of MB adsorbed in the porous PY-GP4 geopolymer adsorbent in these experimental conditions reaches 63.7 mg/g.

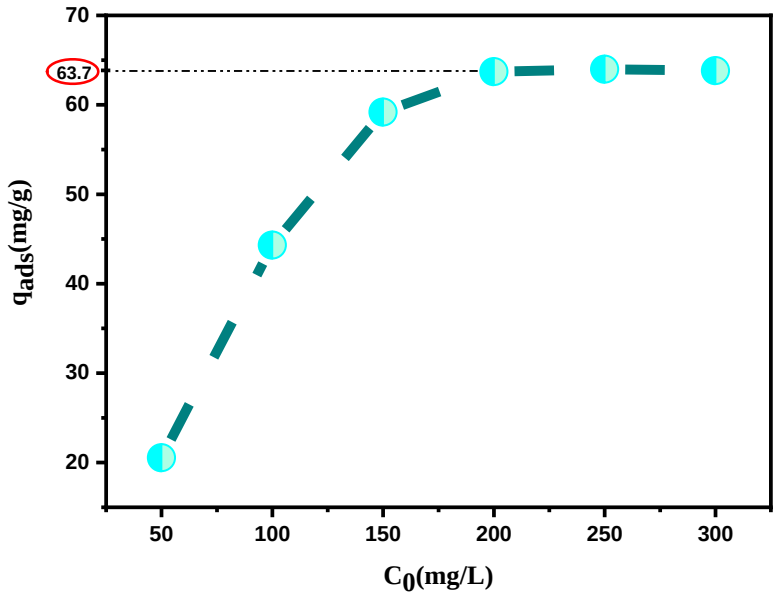

Fig. 9: Effect of the initial dye concentration on the MB adsorption within the porous PY-GP4 geopolymer adsorbent (experimental conditions: [adsorbent] = 2.4 g/L, stirring time = 120 min, temperature = 25 °C and pH = 7).

b- Isotherm Models

Several physical models have been evaluated to understanding the types of interactions between the porous geopolymer adsorbent and the MB cationic dye adsorbate. We have used three conventional models namely, Langmuir, Freundlich and Temkin to test this behavior. The linear equations for these models are presented in the equations 8, 9 and 10 respectively (Acisli et al., 2020).

$$\frac{C_e}{q_e} = \frac{C_e}{q_m} + \frac{1}{K_L\, q_m} \qquad \textbf{(8)}$$

$$\ln q_e = \frac{1}{n} \ln C_e + \ln K_F \qquad \textbf{(9)}$$

$$q_e = B_T \ln K_T + B_T \ln C_e \qquad \textbf{(10)}$$

where q_m (mg.g^{-1}), q_e (mg.g^{-1}) are the maximum and equilibrium adsorption amounts, respectively. C_e and n are the equilibrium concentration and Freundlich coefficient, respectively. In addition, K_L (L.mg^{-1}), K_F (mg$^{1-1/n}$.g^{-1}.L$^{1/n}$), K_T (KJ.mol^{-1}), are the Langmuir, Freundlich and Temkin constants, respectively, and B_T is the constant related to the heat of adsorption.

Table 9 presents the calculated parameters characterizing the isotherm from each model. According to the linear correlation coefficients obtained for the three theoretical models applied, the Langmuir model (R^2 = 0.999) exhibits the best correlation to the MB adsorption in the porous PY-GP4 geopolymer material. This result confirms the heterogeneity of the adsorption sites of this newly developed system. In addition, the maximum adsorption capacity estimated by Langmuir model of 64.10 mg/g is very close of experimentally measured value of 63.70 mg/g. This important result indicates that this porous geopolymer network exhibits surface area and porous volume characteristics in strong agreement with the BET and SEM results. Although the adsorption mechanism of MB molecules on porous geopolymers systems has been proposed by several authors (Siyal et al., 2018; Bouna et al., 2020), this work conclusively shows that MB adsorbed is facilitated by ionic bonds formed between the positively charged MB and the negatively charged geopolymer surface, and by hydrogen bonds between hydroxyl groups (–OH) on the geopolymer pore surface and a nitrogen positions in the MB molecular structure (Siyal et al., 2018; Bouna et al., 2020). Table 10 presents and compares the adsorption capacity of the cationic MB dye by various geopolymer adsorbents reported in the literature.

Table 9: Characteristics parameters calculated for diver isotherms models in the adsorption of MB dye onto PY-GP4 porous geopolymer adsorbent.

Isotherm models	Parameters	
Langmuir	R^2	0.999
	K_L(L.mg^{-1})	1.418
	q_m (mg.g^{-1})	64.103
	q_e^{exp} (mg/g)	63.700
Freundlich	R^2	0.611
	K_F (mg$^{1-1/n}$.g^{-1}.L$^{1/n}$)	34.329
	n	6.849
Temkin	R^2	0.723
	K_T (L.mg^{-1})	6.150
	B_T (KJ.mol^{-1})	443.977

Table 10: Adsorption capacity of MB cationic dye of diver geopolymers materials reveled in literature.

Geopolymer materiel	Adsorbate	q_{max} (mg/g)	Reference
Biomass fly ash based geopolymer spheres	MB	30.1	(Novais et al., 2019)

Biomass fly ash geopolymer monoliths	MB	20.5	(Novais et al., 2018)
Kaolin geopolymer	MB	25.6	(Yousef et al., 2009)
Metakaolin based geopolymer	MB	43.48	(El Alouani et al., 2019)
Metakaolin and rice husk based geopolymer	MB	4.9	(Khan et al., 2015)
PY-GP4 porous geopolymer based pyrophyllite	MB	64.10	This work

4.4 Thermodynamic Study

The thermodynamics parameters namely, enthalpy (ΔH°), entropy (ΔS°) and free energy (ΔG°) were studied in 298 - 328 K temperature interval. That allow determining the adsorption process type. The latest were determined by following equations (11), (12) and (13) mentioned below (Amjlef et al., 2021; Chen et al., 2021):

$$\Delta G° = -RTlnK_d \quad (11)$$

$$\Delta G° = \Delta H° - T\Delta S° \quad (12)$$

$$LnK_d = \frac{-\Delta H°}{RT} + \frac{\Delta S°}{R} \quad (13)$$

Where: K_d is the equilibrium constant, R is the ideal gas constant (8.314 J/K.mol) and T is the temperature (K).

Fig. 10 (a) illustrates the adsorbed amount of MB adsorbate molecules onto our porous geopolymer elaborate at diver temperature. The curve obtained shows that the adsorbed amount increases from 43.27 to 44.21 mg/g with increasing of the temperature from 298 to 373 K. This result indicate that the adsorption process is supporting by temperature medium. The plotting of ln K_d as a function of 1/T is presented in Fig. 10 (b), the thermodynamic parameters enthalpy (ΔH°) and entropy (ΔS°) can be calculated from slop and intercept, respectively. Table 11 presents the thermodynamic parameters calculated. The analysis of the results obtained indicate that the adsorption of MB cationic dye on our porous geopolymer powder is spontaneous (ΔG°<0) in 298 - 328 K temperature range. Moreover, the ΔG° value decrease with increasing of the temperature he passes from -6.49 to -10.61 KJ.mol^{-1} that indicate the adsorption process is more favorite at high temperature. Furthermore, the positive and important value of ΔH° (34 KJ.mol^{-1}) indicates that is an endothermic chemisorption process while the positive value of

ΔS° (0.135 KJ.mol^{-1}K^{-1}) indicates the adsorption process is irreversible (Panda et al., 2018; Siyal et al., 2018).

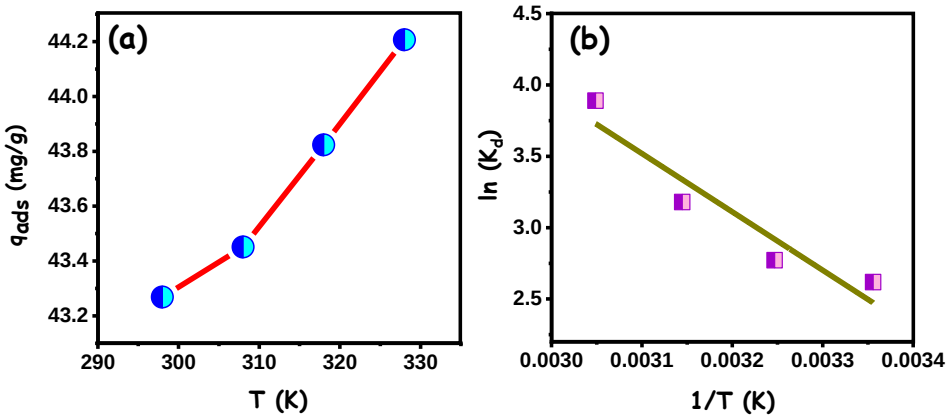

Fig 10. (a) Temperature Effect of adsorption of MB adsorbate dye onto PY-GP4 porous geopolymer adsorbent, **(b)** Van't Hoff plot (Experiments conditions: [adsorbent] = 2.4 g/L, [MB] = 100 mg/g, stirring time = 120 min and pH = 7).

Table 11: Thermodynamic parameters of adsorption of MB adsorbate dye onto PY-GP4 porous geopolymer adsorbent.

T(K)	ΔG (KJ.mol^{-1})	ΔH (KJ.mol^{-1})	ΔS° (KJ.mol^{-1}. K^{-1})
298	-6,486	34,998	0,135
308	-7,098		
318	-8,404		
328	-10,607		

5. Discussion

We have successively characterized the natural Moroccan clay collected from Addis village in the Tata region, located geologically in western part of Bani Mountain south of the Anti-Atlas massif. The XRD results revealed that this natural clay was rich in the pyrophyllite mineral clay and was associated with minor amounts of muscovite and kaolinite clays and the quartz mineral (Fig. 2). Also, the ^{29}Si MAS NMR spectra realized on PY raw clay show an intense signal at ~–96 ppm Q^4(1Al) associate to pyrophyllite clay (Fig. 3(a)). while the signals at ~–108 and ~–112 ppm correspond to the fully condensed Q^4(0Al) Si species of quartz and amorphous silica, respectively, which are present in the raw sample. The ^{29}Si broad resonances in the –80 - –95 ppm range are contributions from Q^3(0Al) (~–93 ppm) of hydroxylated kaolinite and at ~–86 ppm represents Q^3(1Al) and Q^3(2Al) species associated with a muscovite

phase present in the raw material. For ^{27}Al MAS NMR (Figs. 3(b) and 3(c)), we show four coordinate AlO_4 positions attribute to the muscovite phase and six coordinate AlO_6 positions associated with the kaolinite, muscovite and pyrophyllite phases.

The TGA/DTA thermal results of raw PY clay (Fig. 5) shows the presence of two endothermic transitions. The first (observed over the 50-110 °C range) is associated with a mass loss of 2.2% and corresponds to the removal of physisorbed water from the particle surfaces and pore structure of the clay minerals, while the second endothermic transition (appearing over the 420-915 °C range) associated with a mass loss of 5.5% is attributed to dehydroxylation of the pyrophyllite, kaolinite and muscovite clays minerals present in raw sample.

For PY-800 calcined sample, the meta-pyrophyllite phase has been achieved upon calcination at 800 °C. XRD results (Fig. 2) show that the characteristic (003) reflection of pyrophyllite appearing at 29.08° (2θ) which moves to a smaller angle 28.7° (2θ), disappearance of the kaolinite reflections which exhibits reduced crystallinity under thermal treatment due to structural disorder induced by high temperature dehydroxylation of this system. the muscovite was transformed to potassium aluminum silicate phase. The ^{29}Si and ^{27}Al MAS NMR data from the PY-800 sample exhibits clear evidence of dehydroxylation under this thermal treatment. The ^{29}Si resonance at ~–96 ppm of pyrophyllite shifts to ~–102 ppm (see Fig. 3(a)), while the appearance of five coordinate (AlO_5) pyrophyllite resonance at δ_{iso} ~25 ppm (C_Q = 10.5 MHz, η_Q = 0.0) resulting from the $AlO_5(OH) \rightarrow AlO_5$ generated by the pyrophyllite dehydroxylation process (Figs. 3(b) and (c)). The thermal transformation process also induces an increase in AlO_4 speciation at the expense of AlO_6 inventory from the clay compositions. For FTIR results (Fig. 4), the moderately intense band at 3650 cm^{-1} appearing in the raw PY spectrum is characteristic the of OH vibrations associated with pyrophyllite, muscovite and kaolinite clays; this band disappears from PY-800 sample under calcination at 800 °C.

For PY-GP4, elaborate geopolymer, the important value adsorbed by MB reach 64.1 mg/g confirms the porous character of elaborate materials. This is exposed by the SEM images (Figs. 7-e and 7-f) which show certain pores developed on the surface of material as well as by the important values of the specific surface area and the porous volume S_{BET} = 86 m^2/g and Vp = 0.08 cm^3/g respectively, obtained by the adsorption of N_2 (Fig. 6 and Table 6). The amorphous character of our elaborate geopolymer PY-GP4 is highlighted by amorphous bump observed by XRD analysis (Fig. 2), by broadband appears in FTIR spectrum in the 2800-3750 cm^{-1} range characteristic of OH vibrations of amorphous geopolymers (Fig. 4), by SEM images (Figs. 7-e

and 7-f) and by $Q^4(2Al)$, $Q^4(3Al)$ and $Q^4(4Al)$ species showed in ^{29}Si MAS NMR spectrum (Fig. 3(a)) are intrinsic to the amorphous geopolymer network.

Finally, for PY-GP4@MB the sample recovered after adsorption of MB process. The retention of MB molecules by the prepared geopolymer is confirmed by FTIR analysis (Fig. 4) by the presence of bands at 1342, 1387, 1503 and 1607 cm^{-1} attributable to the bending vibrations of MB molecule adsorbed into geopolymer surface as well as by the EDS analysis (Table 7) which shows a significant content of C and S elements correspond to the MB molecules.

Conclusion

We used the natural pyrophyllite clay rich in this study for preparing a porous geopolymer systems. The XRD and NMR (^{29}Si and ^{27}Al) results shows that the contribution of pyrophyllite in geopolymerization reaction was very low, the geopolymer matrix formed was majority assured by alkaline activation of the metakaolin present in the sample. The pyrophyllite role is forming of disordered and heterogeneous geopolymer promote the pore creation. Several geopolymers specimens have been synthesized by varying the concentration of the Si and Na precursors used for preparing the alkaline activation solutions. In particular, PY-GP4 is a geopolymer system synthesized at 70 °C with a lower concentration of the Si and Na chemical precursors. For this system both the specific surface area (S_{BET}) and pore volume (Vp) (S_{BET} = 86 m^2/g and Vp = 0.08 cm^3/g) have increased considerably compared to raw clay (S_{BET} = 30 m^2/g and Vp = 0.05 cm^3/g). This new porous geopolymer system has been utilized for the adsorption and removal of methylene blue (MB) representing a cationic model dye in aqueous media. The results obtained indicate that adsorption kinetics follows a Pseudo Second Order (PSO) model, and the adsorption mechanism was better represented by a Langmuir model compared to Freundlich and Temkin models. These results suggest that an effective heterogeneity of adsorption sites have developed within the network of these new porous geopolymer systems. The thermodynamics experiments show that the overall MB adsorption process is spontaneous, irreversible and represents endothermic chemisorption. The quantity of MB molecules retained by these porous geopolymer systems reaches 64.10 mg/g.

References

Ömer Şahin, Mustafa Kaya, Cafer Saka. Applied Clay Science. Plasma-surface modification on bentonite clay to improve the performance of adsorption of methylene blue. 116–117 (2015) 46–53

Acisli, O., Acar, I., Khataee, A., 2020. Preparation of a fly ash-based geopolymer for removal of a cationic dye: Isothermal, kinetic and thermodynamic studies. J. Ind. Eng. Chem. 83, 53–63.

Ait El Fakir, A., Anfar, Z., Amedlous, A., Amjlef, A., Farsad, S., Jada, A., El Alem, N., 2021. Synergistic effect for efficient catalytic persulfate activation in conducting polymers-hematite sand composites: Enhancement of chemical stability. Appl. Catal. A Gen. 623, 118246.

Akhsassi, B., Bouddouch, A., Naciri, Y., Bakiz, B., Taoufyq, A., Favotto, C., Villain, S., Guinneton, F., Benlhachemi, A., 2021. Enhanced photocatalytic activity of Zn3(PO4)2/ZnO composite semiconductor prepared by different methods. Chem. Phys. Lett. 783, 139046.

Amjlef, A., Khrach, S., Ait El Fakir, A., Farsad, S., Et-Taleb, S., El Alem, N., 2021. Adsorptive properties investigation of natural sand as adsorbent for methylene blue removal from contaminated water. Nanotechnol. Environ. Eng. 6, 26.

Bouddouch, A., Amaterz, E., Bakiz, B., Taoufyq, A., Guinneton, F., Villain, S., Gavarri, J.R., Valmalette, J.C., Benlhachemi, A., 2021. Customized synthesis of functional bismuth phosphate using different methods: photocatalytic and photoluminescence properties enhancement. Nanotechnol. Environ. Eng. 6, 1–12.

Bouna, L., Ait El Fakir, A., Benlhachemi, A., Draoui, K., Ezahri, M., Bakiz, B., Villain, S., Guinneton, F., Elalem, N., 2020. Synthesis and characterization of mesoporous geopolymer based on Moroccan kaolinite rich clay. Appl. Clay Sci. 196, 105764.

Bradley, S.M., Hanna, J. V., 1994. 27Al and 23Na MAS NMR and powder x-ray diffraction studies of sodium aluminate speciation and the mechanistics of aluminum hydroxide precipitation upon acid hydrolysis. Journal of the American Chemical Society. 116, 7771-7783.

Bradley, S.M., Hanna, J. V., 1993. Aluminium-27 MAS NMR investigations of sodium aluminates formed from high pH solutions: Evidence of a complex polymer containing both four- and six-coordinate aluminium. J. Chem. Soc. Chem. Commun. 120, 1249–1251.

Brunauer, S., Emmett, P.H., Teller, E., 1938. Adsorption of Gases in Multimolecular Layers. J. Am. Chem. Soc. 60, 309–319.

Chen, Y., Tang, J., Wang, S., Zhang, L., Sun, W., 2021. Bimetallic coordination polymer for highly selective removal of Pb(II): Activation energy, isosteric heat of adsorption and adsorption mechanism. Chem. Eng. J. 425, 131474.

Darmayanti, L., Kadja, G.T.M., Notodarmojo, S., Damanhuri, E., 2019. Structural alteration within fly ash-based geopolymers governing the adsorption of Cu^{2+} from aqueous environment : Effect of alkali activation. J. Hazard. Mater. 377, 305–314.

Davidovits, J., 1991. Geopolymers. J. Therm. Anal. 37, 1633–1656.

Dzoujo, H.T., Shikuku, V.O., Tome, S., Akiri, S., Kengne, N.M., Abdpour, S., Janiak, C., Etoh, M.A., Dina, D., 2022. Synthesis of pozzolan and sugarcane bagasse derived geopolymer-biochar composites for methylene blue sequestration from aqueous medium. J. Environ. Manage. 318, 115533

El Alouani, M., Alehyen, S., El Achouri, M., Taibi, M., 2019. Preparation, Characterization, and Application of Metakaolin-Based Geopolymer for Removal of Methylene Blue from Aqueous Solution. J. Chem. 4212901.

El Gaidoumi, A., Doña Rodríguez, J.M., Pulido Melián, E., González-Díaz, O.M., Navío Santos, J.A., El Bali, B., Kherbeche, A., 2019. Synthesis of sol-gel pyrophyllite/TiO2 heterostructures: Effect of calcination temperature and methanol washing on photocatalytic activity. Surfaces and Interfaces 14, 19–25.

Erdemoğlu, M., Birinci, M., Uysal, T., 2020. Thermal Behavior of Pyrophyllite Ore during Calcination for Thermal Activation for Aluminum Extraction by Acid Leaching. Clays Clay Miner. 68, 89–99.

Erdemoğlu, M., Erdemoğlu, S., Sayilkan, F., Akarsu, M., Şener, Ş., Sayilkan, H., 2004. Organo-functional modified pyrophyllite: Preparation, characterisation and Pb(II) ion adsorption property. Appl. Clay Sci. 27, 41–52.

Fitzgerald, J.J., Hamza, A.I., Dec, S.F., Bronnimann, C.E., 1996. Solid-State 27 Al and 29 Si

NMR and 1 H CRAMPS Studies of the Thermal Transformations of the 2 : 1 Phyllosilicate Pyrophyllite. J. Phys. Chem. 3654, 17351–17360.

Ge, Y., Cui, X., Kong, Y., Li, Z., He, Y., Zhou, Q., 2015. Porous geopolymeric spheres for removal of Cu(II) from aqueous solution: Synthesis and evaluation. J. Hazard. Mater. 283, 244–251.

Ge, Y., Cui, X., Liao, C., Li, Z., 2017. Facile fabrication of green geopolymer/alginate hybrid spheres for efficient removal of Cu(II) in water: Batch and column studies. Chem. Eng. J. 311, 126–134.

Guanghui, Z, J., Luo, J., Liu, M., Jiang, T., Qiu, G., 2014. Thermal transformation of pyrophyllite and alkali dissolution behavior of silicon. Appl. Clay Sci. 99, 282–288.

He, P.Y., Zhang, Y.J., Chen, H., Han, Z.C., Liu, L.C., 2020. Low-cost and facile synthesis of geopolymer-zeolite composite membrane for chromium(VI) separation from aqueous solution. J. Hazard. Mater. 392, 122359.

Hermann, D.T., Tome, S., Shikuku, V.O., Tchuigwa, J.B., Spieß, A., Janiak, C., Etoh, M.A., Joh Dina, D.D., 2021. Enhanced Performance of Hydrogen Peroxide Modified Pozzolan-Based Geopolymer for Abatement of Methylene Blue from Aqueous Medium. Silicon.

Hu, S., Zhong, L., Yang, X., Bai, H., Ren, B., Zhao, Y., Zhang, W., Ju, X., Wen, H., Mao, S., Tao, R., Li, C., 2020. Synthesis of rare earth tailing-based geopolymer for efficiently immobilizing heavy metals. Constr. Build. Mater. 254, 119273.

Harris, R. K., Becker, E.D., Menezes, S.M.C. de, Goodfellow, R., Granger, P., 2002. NMR nomenclature: nuclear spin properties and conventions for chemical shifts. IUPAC Recommendations, 2001. Solid State Nucl. Magn. Reson. 22, 458–483.

Khan, M.I., Min, T.K., Azizli, K., Sufian, S., Ullah, H., Man, Z., 2015. Effective removal of methylene blue from water using phosphoric acid based geopolymers: Synthesis, characterizations and adsorption studies. RSC Adv. 5, 61410–61420.

Kim, B., Lee, J., Kang, J., Um, W., 2021. Development of geopolymer waste form for immobilization of radioactive borate waste. J. Hazard. Mater. 419, 126402.

Lertcumfu, N., Jaita, P., Thammarong, S., Lamkhao, S., Tandorn, S., Randorn, C., Tunkasiri, T., Rujijanagul, G., 2020. Influence of graphene oxide additive on physical, microstructure, adsorption, and photocatalytic properties of calcined kaolinite-based

geopolymer ceramic composites. Colloids Surfaces A Physicochem. Eng. Asp. 602, 125080.

Li, G., Zeng, J., Luo, J., Liu, M., Jiang, T., Qiu, G., 2014. Thermal transformation of pyrophyllite and alkali dissolution behavior of silicon. Appl. Clay Sci. 99, 282–288.

Longhi, A., Rodríguez, E.D., Walkley, B., Zhang, Z., Paula, A., 2020. Metakaolin-based geopolymers : Relation between formulation , physicochemical properties and efflorescence formation. Composites Part B: Engineering. 182, 107671182.

Mackenzie, K., Smith, M.E., 2002. Multinuclear Solid-State Nuclear Magnetic Resonance of Inorganic Materials. Pergaman Materials Series, Vol. 4, Pergamon Press, Oxford, 218.

Massiot, D., Fayon, F., Capron, M., King, I., Le Calvé, S., Alonso, B., Durand, J.O., Bujoli, B., Gan, Z., Hoatson, G., 2002. Modelling one- and two-dimensional solid-state NMR spectra. Magn. Reson. Chem. 40, 70–76.

Niu, X., Elakneswaran, Y., Islam, C.R., Provis, J.L., Sato, T., 2022. Adsorption behaviour of simulant radionuclide cations and anions in metakaolin-based geopolymer. J. Hazard. Mater. 429, 128373.

Novais, R.M., Ascensão, G., Tobaldi, D.M., Seabra, M.P., Labrincha, J.A., 2018. Biomass fly ash geopolymer monoliths for effective methylene blue removal from wastewaters. J. Clean. Prod. 171, 783–794.

Novais R.M., Carvalheiras J., Tobaldi D.M., Seabra M.P., Pullar R.C., Labrincha J.A., 2019. Synthesis of porous biomass fly ash-based geopolymer spheres for efficient removal of methylene blue from wastewaters. J. Clean. Prod. 207, 350–362.

Novais, R.M., Pullar, R.C., Labrincha, J.A., 2020. Geopolymer foams: An overview of recent advancements. Progress in Materials Science. 109, 100621.

Panda, L., Rath, S.S., Rao, D.S., Nayak, B.B., Das, B., Misra, P.K., 2018. Thorough understanding of the kinetics and mechanism of heavy metal adsorption onto a pyrophyllite mine waste based geopolymer. J. Mol. Liq. 263, 428–441.

Pérez-Maqueda, L.A., Montes, O.M., González-Macias, E.M., Franco, F., Poyato, J., Pérez-Rodríguez, J.L., 2004. Thermal transformations of sonicated pyrophyllite. Appl. Clay Sci. 24, 201–207.

Rowles, M.R., Hanna, J. V., Pike, K.J., Smith, M.E., O'Connor, B.H., 2007. 29Si, 27Al, 1H and 23Na MAS NMR study of the bonding character in aluminosilicate inorganic polymers. Appl. Magn. Reson. 32, 663–689.

Sa´nchez-Soto, P.J., Pe´rez-Rodrı´guez, J., 1997. Influence of Grinding in Pyrophyllite - Mullite Thermal Transformation Assessed by 29 Si and 27 Al MAS NMR Spectroscopies 4756, 677–684.

Sainchez-soto, P.J., Sobrados, I., Sam, J., Perez-rodr, J.L., 1993. 29-Si and 27-A1 Magic-Angle Spinning Nuclear Magnetic Resonance Study of the Thermal Transformations of Pyrophyllite. J Am Ceram Soc 28, 3024–3028.

Samuel, D.M., Sutrisno, A., Kriven, W.M., 2021. Relative importance of Al (V) and reinforcement to the flexural strength of geopolymer composites. J. Am. Ceram. Soc. 3452–3460.

Sanz, J., Serratosa, J.M., 1984. 29Si and 27Al High-Resolution MAS-NMR Phyllosilicates. J. Am. Chem. Soc. 4790–4793.

Sayed, M., Gado, R.A., Naga, S.M., Colombo, P., Elsayed, H., 2020. Influence of the thermal treatment on the characteristics of porous geopolymers as potential biomaterials. Mater. Sci. Eng. C 116, 111171.

Sing, k. S.W., Everett, d. H., Haul, r. A.W., Moscou, L., Pierotti, r. A., Rouquerol, J., Siemieniewska, T., 1985. Reporting physisorption data for gas/solid systems with special reference to the determination of surface area and porosity. Int. union pure Appl. Chem. 6, 710–713.

Singhal, A., Gangwar, B.P., Gayathry, J.M., 2017. CTAB modified large surface area nanoporous geopolymer with high adsorption capacity for copper ion removal. Appl. Clay Sci. 150, 106–114.

Siyal, A.A., Shamsuddin, M.R., Khan, M.I., Rabat, N.E., Zulfiqar, M., Man, Z., Siame, J., Azizli, K.A., 2018. A review on geopolymers as emerging materials for the adsorption of heavy metals and dyes. J. Environ. Manage. 224, 327–339.

Su, Q., Deng, L., Ye, Q., He, Y., Cui, X., 2020. KOH-activated geopolymer microspheres recycle Co(II) with higher adsorption capacity than NaOH-activated ones. ACS Omega 5, 23898–23908.

Tchakouté, H.K., Bewa, C.N., Fotio, D., Dieuhou, C.M., Kamseu, E., Rüscher, C.H., 2021. Influence of alumina on the compressive strengths and microstructural properties of the acid-based geopolymers from calcined indurated laterite and metakaolin. Appl. Clay Sci. 209, 106148.

Tian, Q., Guo, B., Sasaki, K., 2020. Immobilization mechanism of Se oxyanions in geopolymer: Effects of alkaline activators and calcined hydrotalcite additive. J. Hazard. Mater. 387, 121994.

Tsai, Y.L., Hanna, J. V., Lee, Y.L., Smith, M.E., Chan, J.C.C., 2010. Solid-state NMR study of geopolymer prepared by sol-gel chemistry. J. Solid State Chem. 183, 3017–3022.

Walkley, B., Rees, G.J., Nicolas, R.S., Deventer, J.S.J. van, Hanna, J. V., Provis, J.L., 2018. New Structural Model of Sodium Aluminosilicate Gels and the Role of Charge Balancing. J. Phys. Chem. A 122, 5673–5685.

Wan, Q., Rao, F., Song, S., 2017. Reexamining calcination of kaolinite for the synthesis of metakaolin geopolymers - roles of dehydroxylation and recrystallization. J. Non. Cryst. Solids 460, 74–80.

Watanabe, T., Shimizu, H., Nagasawa, K., Masuda, A., Saito, H., 1987. ^{29} Si- and ^{27} Al-MAS/NMR study of the thermal transformations of kaolinite. Clay Miner. 22, 37–48.

Weiss, C.A., Altaner, S.P., Kirkpatrick, R.J., 1987. High-resolution 29Si NMR spectroscopy of 2:1 layer silicates: correlations among chemical shift, structural distortions, and chemical variations. Am. Mineral. 72, 935–942.

Yousef, R.I., El-Eswed, B., Alshaaer, M., Khalili, F., Khoury, H., 2009. The influence of using Jordanian natural zeolite on the adsorption, physical, and mechanical properties of geopolymers products. J. Hazard. Mater. 165, 379–387.

Zhang, J., Yan, J., Sheng, J., 2015. Dry grinding effect on pyrophyllite-quartz natural mixture and its influence on the structural alternation of pyrophyllite. Micron 71, 1–6.

Zhang, M., El-Korchi, T., Zhang, G., Liang, J., Tao, M., 2014. Synthesis factors affecting mechanical properties, microstructure, and chemical composition of red mud-fly ash based geopolymers. Fuel 134, 315–325.